

Received 4 June 2024, accepted 26 July 2024, date of publication 30 July 2024, date of current version 7 August 2024.

Digital Object Identifier 10.1109/ACCESS.2024.3435698

## RESEARCH ARTICLE

# Nonlinear Control of Ship-Mounted Rotary Crane Based on Adaptive Dynamic Programming

HUAN XI<sup>ID</sup>, (Member, IEEE), QIANGYING WU, AND HUIMIN OUYANG<sup>ID</sup>, (Senior Member, IEEE)

College of Electrical Engineering and Control Science, Nanjing Tech University, Nanjing 211816, China

Corresponding author: Huimin Ouyang (ouyang1982@njtech.edu.cn)

This work was supported by the National Natural Science Foundation of China under Grant 61703202.

**ABSTRACT** As a crucial component in marine transportation, the precision of ship-mounted rotary cranes directly impacts the efficiency and safety of lifting operations. However, the inability to directly control the swing angle of the load through the drive mechanism renders ship-mounted rotary cranes inherently complex, featuring underactuated and coupled characteristics. In this study, we propose an optimal feedback controller leveraging adaptive dynamic programming (ADP), which integrates sliding mode control with optimal control strategies. Specifically, we devise a judicious cost function and solve the Hamilton-Jacobi-Bellman (HJB) equation using the adaptive dynamic programming approach. Subsequently, the optimal feedback controller is derived through iterative batch neural network training facilitated by the adaptive update algorithm. Moreover, we establish the stability of the proposed controller through rigorous Lyapunov techniques and LaSalle's invariance principle. Experimental validation confirms the efficacy of our approach, highlighting its practical utility in real-world scenarios.

**INDEX TERMS** Underactuated systems, adaptive dynamic programming, motion control, vibration control.

## I. INTRODUCTION

The ship-mounted rotary crane stands as a pivotal component within the modern maritime industry, serving primarily for the lifting and transportation of large-scale materials. With the rapid advancement of shipbuilding practices, the demand for heightened performance and control precision in marine rotating cranes has surged. Functioning as precision-centric lifting apparatus, ship-mounted rotary cranes necessitate attributes of superior stability, precision, and safety. Diverging from their land-based counterparts, ship-mounted rotary cranes confront an array of intricate operational environments, including wind, waves, currents, tides, and other natural variables, alongside vessel movement and load lifting conditions. These environmental nuances profoundly influence the operational efficacy and safety performance of rotary cranes at sea. Consequently, investigating the control mechanisms of marine rotating cranes assumes paramount importance, carrying significant practical implications and application value. Moreover, the unique operational dynamics of ship-mounted rotary cranes present distinctive

challenges. As the crane's load can only be tethered to the cantilever via a rope, and the crane's driving mechanism lacks direct control over load swing, the system manifests intricate underactuated characteristics. When compounded by the complexities of fluctuating waves and wind perturbations, the control of ship-mounted rotary cranes becomes an intricate endeavor. Furthermore, in certain operational scenarios, solely relying on the cantilever for load positioning may prove inadequate, necessitating consideration for variable rope length. Unlike their fixed-rope-length counterparts, variable-rope-length cranes witness fluctuations in the inherent frequency of the load swing subsystem, engendering intricate system dynamics oscillating between drive/underdriven and drive/torque configurations.

In recent decades, many effective control methods have been proposed for underactuated systems [1], [2]. Among them, open-loop control [3], [4] is a focus of research, which mainly includes input shaping [5], [6] and trajectory planning [7], [8]. Furthermore, the actual system is usually affected by external perturbations as well as internal instability factors, and simple open-loop control cannot fully meet the control requirements, so the stability of the whole system can be improved by the closed loop control [9], [10],

The associate editor coordinating the review of this manuscript and approving it for publication was Jingang Jiang<sup>ID</sup>.

such as sliding mode control [11], [12], adaptive control [13], MPC control [14], and robust control [15], [16]. Optimal control [17], [18], [19] of nonlinear systems has developed rapidly in recent years. In general, optimal control requires the solution of HJB equations, which are relatively easy to solve for linear systems, but the solution of nonlinear partial differential equations in nonlinear systems has been an urgent problem.

To solve the problem with unknown parameters and dynamic uncertainty, Jiang and Jiang [20] designed a decentralized optimal controller by combining robust control with policy iteration techniques. In [21], the GFHM policy iteration algorithm is used to solve the approximate solution of the coupled Hamilton-Jacobi-Bellman equations for the optimal coordinated control of multiple intelligence. In [22], a model-free distributed controller for multiple intelligence was designed to achieve perturbation suppression and asymptotic stabilization of each follower using online input and state data. Ming et al. [23] achieved optimal tracking of a discrete system through a new static triggering mechanism by sampling and updating the control signal. In [24], a RAOTC (robust adaptive optimal tracking control) method combining adaptive control, robust control and optimal control is presented to achieve the stabilization of transient tracking error dynamics and verify the effectiveness through experiments. Zhao et al. [25] reconstructed the unpredictable states of the system through an input-output redefinition method, proposed an optimal method combining triggered output feedback and adaptive control, and successfully applied it to a multi-machine power system. Liu et al. [26] successfully applied ADP to a complex traffic light system and optimized the traffic light operation method. Wang et al. [27] transformed the current distribution and voltage regulation into an optimization problem, and proposes an efficient voltage and current regulation method for wind/solar hybrid systems based on Bellman's distributed adaptive dynamic planning, which achieves the optimization of the control objective. Tang et al. [28] approximated the optimal solution of the HJB equations by a critical neural network and realized the steady-state control of the hypersonic gliding vehicle using the dynamic surface control (DSC) method. Dong et al. [29] designed a sliding mode optimal approximation law using ADP to constrain the reduced-order system dynamics in the desired region, and implemented a tracking control method for n-links robots under parameter uncertainty, time profile failure, and input saturation constraints. In [30], the researchers simplified the dimensions of the problem by dividing the energy management problem of a hybrid vehicle into the scheduling problems of the engine and the motor, and proposed an energy scheduling method for a hierarchically operated vehicle with switching capabilities. Na et al. [31] proposed a new optimal control method by estimating the modelling uncertainty of the wave-energy converter through a new estimator with a simple structure combined with robust control. Wang et al. [32] measured the inputs and outputs of the system by means

of an observer and proposed a new ADP method based on the principle of internal model principle, which was finally experimentally verified on a grid-connected LCL inverter system.

The preceding research elucidates a prevailing trend: a plethora of studies have delved into optimal control methodologies for linear systems featuring low dimensions. However, the formidable challenge persists in tackling the control intricacies of ship-mounted rotary cranes. These systems are emblematic of underactuation, robust coupling, and nonlinearity, compounded by the imperative to contend with input constraints and uncertain external wave perturbations. Addressing these multifaceted challenges remains an exigent task necessitating immediate attention and resolution.

This paper delves into the control quandary posed by ship-mounted rotary cranes with external perturbations, presenting an adaptive learning sliding mode controller as a viable solution. Through the integration of driveable and underdriven state variables, the system's state equations are reformulated into standard state-space form, facilitating the construction of a novel HJB equation. Diverging from conventional ADP algorithms necessitating both action and critic neural networks, our approach mandates solely a critic neural network. Leveraging an adaptive algorithm update, the approximate optimal control can be attained efficiently. The proposed methodology's stability is rigorously established through theoretical frameworks employing Lyapunov techniques and LaSalle's invariance principle. Subsequently, robust validation is carried out by an experimental platform to demonstrate the relevance of this paper's method for real-world applications.

The main contributions of this paper are as follows:

- 1) Diverging from existing models, this paper meticulously considers the impact of continuous yaw, roll, and heave disturbances on ship-mounted rotary cranes. It achieves this by adeptly transforming the prevailing dynamical model into a standard state-space form through the strategic coupling of state variables.
- 2) This paper amalgamates optimal control with sliding mode control theory to achieve dual objectives: ensuring precise load displacement and eliminating pendulum angle deviations, all while effectively mitigating external perturbations.
- 3) The stability of the proposed controller is rigorously substantiated through Lyapunov techniques and LaSalle's invariance principle, underscoring its robustness in dynamic scenarios. Furthermore, the efficacy of the proposed method is empirically validated through meticulous experimentation.

## II. PROBLEM STATEMENT

In this section, we first model the dynamics of the ship-mounted rotary crane. The original mathematical model of the ship-mounted rotary crane does not conform to the standard form of adaptive dynamic programming. Therefore we made some reasonable transformations to the

mathematical model of the crane, the underactuated part of the system is first coupled to the actuated part of the system by state transformation, and then the coupled system model is converted to a state space representation.

### A. MODEL CONSTRUCTION

The ship-mounted rotary crane is modeled as follows [33]:

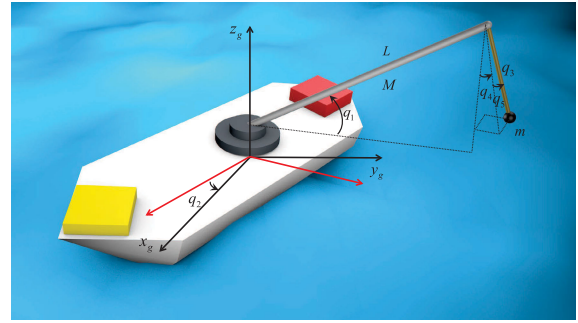


FIGURE 1. Crane model.

$$\begin{aligned}
 c_{31} &= mL S_{1-4} C_5 \dot{q}_1 - mL S_1 S_5 \dot{q}_2, \quad c_{32} = -mq_3 S_4^2 C_5^2 \dot{q}_2 \\
 &\quad - mq_3 S_5^2 \dot{q}_2 - mL C_1 S_4 C_5 \dot{q}_2 - mL S_1 S_5 \dot{q}_1 \\
 &\quad + mq_3 C_4 S_5 C_5 \dot{q}_4 \\
 &\quad - mq_3 S_4 \dot{q}_5, \quad c_{33} = 0, \quad c_{34} = -mq_3 C_5^2 \dot{q}_4 + mq_3 C_4 S_5 C_5 \dot{q}_2, \\
 c_{35} &= -mq_3 \dot{q}_5 - mq_3 S_4 \dot{q}_2, \quad c_{41} = -mL C_{1-4} \dot{q}_1, \\
 c_{42} &= -mq_3^2 S_4 C_4 C_5^2 \dot{q}_2 - mL q_3 C_1 C_4 C_5 \dot{q}_2 - mq_3^2 C_4 C_5^2 \dot{q}_5 \\
 &\quad - mq_3 \dot{q}_3 C_4 S_5 C_5, \quad c_{43} = mq_3 C_5^2 \dot{q}_4 - mq_3 C_4 S_5 C_5 \dot{q}_2, \\
 c_{44} &= mq_3 \dot{q}_3 C_5^2 - mq_3^2 S_5 C_5 \dot{q}_5, \quad c_{45} = -mq_3^2 C_4 C_5^2 \dot{q}_2 \\
 &\quad - mq_3^2 S_5 C_5 \dot{q}_4, \quad c_{51} = -mL q_3 S_{1-4} S_5 \dot{q}_1 - mL q_3 S_1 C_5 \dot{q}_2, \\
 c_{52} &= -mq_3^2 C_4^2 S_5 C_5 \dot{q}_2 + mL q_3 C_1 S_4 S_5 \dot{q}_2 - mL q_3 S_1 C_5 \dot{q}_1 \\
 &\quad + mq_3 \dot{q}_3 S_4 + mq_3^2 C_4 C_5^2 \dot{q}_4, \quad c_{53} = mq_3 S_4 \dot{q}_2 + mq_3 \dot{q}_5, \\
 c_{54} &= mq_3^2 S_5 C_5 \dot{q}_4 + mq_3^2 C_4 C_5^2 \dot{q}_2, \quad c_{55} = mq_3 \dot{q}_3, \\
 g_1 &= (m + \frac{1}{2} M_1) g L C_1, \quad g_2 = 0, \quad g_3 = -mg C_4 C_5, \\
 g_4 &= mg q_3 S_4 C_5, \quad g_5 = mg q_3 C_4 S_5, \tag{1}
 \end{aligned}$$

We abbreviate  $\sin q_j$  and  $\cos q_j$  as  $S_j$  and  $C_j$  ( $j=1,2,3,4,5$ ) for readability, respectively. Detailed parameters are shown in Table 1:

TABLE 1. Parameters of the ship-mounted rotary crane.

Symbols	Descriptions	Physical units
$M$	the mass of the boom	kg
$m$	the mass of the load	kg
$L$	Length of the boom	m
$g$	the acceleration of the gravity	m/s <sup>2</sup>
$q_1$	the luffing angle of the boom	deg
$q_2$	the rotation angle of the boom	deg
$q_3$	the length of the rope	m
$q_4$	the radial swing angles of the load	deg
$q_5$	the tangential swing angles of the load	deg
$\tau_1$	Boom drive torque 1	Nm
$\tau_2$	Boom drive torque 2	Nm
$\tau_3$	Rope driving torque	N

The control input state quantity of the system is 3 and the output state quantity is 5, so the whole system exhibits underactuated characteristics. Next, we performed a partial feedback linearization of the dynamic model of the ship-mounted rotary crane.

Taking a split of Eq. (1), we obtain:

$$M_{11} \ddot{q}_a + M_{12} \ddot{q}_u + C_{11} \dot{q}_a + C_{12} \dot{q}_u + G_a = u_a + d_a \tag{2}$$

$$M_{21} \ddot{q}_a + M_{22} \ddot{q}_u + C_{21} \dot{q}_a + C_{22} \dot{q}_u + G_u = d_u \tag{3}$$

$$\begin{aligned}
 M_s(q) \ddot{q} + C(q, \dot{q}) \dot{q} + G &= \tau + d \\
 M_s &= \begin{bmatrix} m_{11} & m_{12} & m_{13} & m_{14} & m_{15} \\ m_{21} & m_{22} & m_{23} & m_{24} & m_{25} \\ m_{31} & m_{32} & m_{33} & m_{34} & m_{35} \\ m_{41} & m_{42} & m_{43} & m_{44} & m_{45} \\ m_{51} & m_{52} & m_{53} & m_{54} & m_{55} \end{bmatrix}, \\
 C &= \begin{bmatrix} c_{11} & c_{12} & c_{13} & c_{14} & c_{15} \\ c_{21} & c_{22} & c_{23} & c_{24} & c_{25} \\ c_{31} & c_{32} & c_{33} & c_{34} & c_{35} \\ c_{41} & c_{42} & c_{43} & c_{44} & c_{45} \\ c_{51} & c_{52} & c_{53} & c_{54} & c_{55} \end{bmatrix}, \\
 G(q) &= [g_1 \ g_2 \ g_3 \ g_4 \ g_5]^T, \\
 \tau &= [\tau_1 \ \tau_2 \ \tau_3 \ 0 \ 0]^T, \\
 q &= [q_1 \ q_2 \ q_3 \ q_4 \ q_5]^T, \\
 m_{11} &= mL^2 + \frac{1}{3} M_1 L^2, \quad m_{12} = mL q_3 S_1 S_5, \quad m_{13} = -mL C_{1-4} C_5, \\
 m_{14} &= mL q_3 S_{1-4} C_5, \quad m_{15} = mL q_3 C_{1-4} S_5, \quad m_{21} = mL q_3 S_1 S_5, \\
 m_{22} &= \frac{1}{3} M_1 L^2 C_1^2 + mL^2 C_1^2 + mq_3^2 S_4^2 C_5^2 + mq_3^2 S_5^2 \\
 &\quad + 2mL q_3 C_1 S_4 C_5, \quad m_{23} = mL C_1 S_5, \quad m_{24} = -mq_3^2 C_4 S_5 C_5, \\
 m_{25} &= mq_3^2 S_4 + mL q_3 C_1 C_5, \quad m_{31} = -mL C_{1-4} C_5, \\
 m_{32} &= mL C_1 S_5, \quad m_{33} = m, \quad m_{34} = 0, \quad m_{35} = 0, \\
 m_{41} &= mL q_3 S_{1-4} C_5, \quad m_{42} = -mq_3^2 C_4 S_5 C_5, \quad m_{43} = 0, \\
 m_{44} &= mq_3^2 C_5^2, \quad m_{45} = 0, \quad m_{51} = mL q_3 C_{1-4} S_5, \\
 m_{52} &= mq_3^2 S_4 + mL q_3 C_1 C_5, \quad m_{53} = 0, \quad m_{54} = 0, \quad m_{55} = mq_3^2, \\
 c_{11} &= 0, \quad c_{12} = mL^2 S_1 C_1 \dot{q}_2 + mL q_3 S_1 S_4 C_5 \dot{q}_2 \\
 &\quad + \frac{1}{3} M_1 L^2 S_1 C_1 \dot{q}_2 + mL \dot{q}_3 S_1 S_5 + mL q_3 S_1 C_5 \dot{q}_5, \\
 c_{13} &= mL S_1 S_5 \dot{q}_2 - mL S_{1-4} C_5 \dot{q}_4 + mL C_{1-4} S_5 \dot{q}_5, \\
 c_{14} &= mL q_3 C_{1-4} C_5 \dot{q}_4 - mL \dot{q}_3 S_{1-4} C_5 + mL q_3 S_{1-4} S_5 \dot{q}_5, \\
 c_{15} &= mL q_3 C_{1-4} C_5 \dot{q}_5 + mL q_3 S_1 C_5 \dot{q}_2 + mL \dot{q}_3 C_{1-4} S_5 \\
 &\quad + mL q_3 S_{1-4} S_5 \dot{q}_4, \quad c_{21} = -mL^2 S_1 C_1 \dot{q}_2 - mL q_3 S_1 S_4 C_5 \dot{q}_2 \\
 &\quad + mL q_3 C_1 C_5 \dot{q}_1 - \frac{1}{3} M_1 L^2 S_1 C_1 \dot{q}_2, \quad c_{22} = -mL^2 S_1 C_1 \dot{q}_1 \\
 &\quad - \frac{1}{3} M_1 L^2 S_1 C_1 \dot{q}_1 - mL q_3 S_1 S_4 C_5 \dot{q}_1 + mq_3^2 S_4 C_4 C_5^2 \dot{q}_4 \\
 &\quad + mL q_3 C_1 C_4 C_5 \dot{q}_4 + mq_3^2 C_4^2 S_5 C_5 \dot{q}_5 - mL q_3 C_1 S_4 S_5 \dot{q}_5 \\
 &\quad + mq_3 \dot{q}_3 S_4^2 C_5^2 + mq_3 \dot{q}_3 S_5^2 + mL \dot{q}_3 C_1 S_4 C_5, \\
 c_{23} &= mq_3 \dot{q}_2 S_4^2 C_5^2 + mq_3 \dot{q}_2 S_5^2 + mL C_1 S_4 C_5 \dot{q}_2 \\
 &\quad - mq_3 C_4 S_5 C_5 \dot{q}_4 + mL C_1 C_5 \dot{q}_5 + mq_3 S_4 \dot{q}_5, \\
 c_{24} &= mq_3^2 S_4 S_5 C_5 \dot{q}_4 + mq_3^2 S_4 C_4 C_5^2 \dot{q}_2 + mL q_3 C_1 C_4 C_5 \dot{q}_2 \\
 &\quad + mq_3^2 C_4 S_5^2 \dot{q}_5 - mq_3 \dot{q}_3 C_4 S_5 C_5, \quad c_{25} = -mL q_3 C_1 S_5 \dot{q}_5 \\
 &\quad + mq_3^2 C_4^2 S_5 C_5 \dot{q}_2 + mq_3 \dot{q}_3 S_4 - mL q_3 C_1 S_4 S_5 \dot{q}_2 \\
 &\quad + mq_3^2 C_4 S_5^2 \dot{q}_4 + mL \dot{q}_3 C_1 C_5,
 \end{aligned}$$

where  $M_s = \begin{bmatrix} M_{11} & M_{12} \\ M_{21} & M_{22} \end{bmatrix}$ ,  $C = \begin{bmatrix} C_{11} & C_{12} \\ C_{21} & C_{22} \end{bmatrix}$ ,  $G = \begin{bmatrix} G_a \\ G_u \end{bmatrix}$ ,  $q_a = [q_1 \ q_2 \ l]^T$ ,  $q_u = [q_3 \ q_4]^T$ ,  $u_a = [\tau_1 \ \tau_2 \ \tau_3]^T$ .

By means of Eq. (3), it is obtained that:

$$\dot{q}_u = M_{22}^{-1}(-M_{21}\ddot{q}_a - C_{21}\dot{q}_a - C_{22}\dot{q}_u - G_u + d_u) \quad (4)$$

Bringing Eq. (4) into Eq. (2) yields:

$$\bar{M}_1(q)\ddot{q}_a + \bar{C}(q, \dot{q})\dot{q}_a + \bar{G} = \bar{u} + \bar{d} \quad (5)$$

where  $\bar{M}_1(q) = M_{11} - M_{12}M_{22}^{-1}M_{21}$ ,  $\bar{C}(q, \dot{q}) = -M_{12}M_{22}^{-1}C_{21} + C_{11}$ ,  $\bar{G} = (-M_{12}M_{22}^{-1}C_{22} + C_{12})\dot{q}_u - M_{12}M_{22}^{-1}G_u + G_a$ ,  $\bar{u} = u_a$ ,  $\bar{d} = d_a - M_{12}M_{22}^{-1}d_u$ . With the coupling transformations described above, we transform the original form containing underactuated state variables into a form containing only actuable variables.

Through Eq. (5), we can obtain the following state space expressions:

$$\begin{cases} \dot{x}_1 = x_2 \\ \dot{x}_2 = v(q_a, \dot{q}_a) + h(q_a)(\bar{u} + \bar{d}) \\ y = x_1 \end{cases} \quad (6)$$

where  $x_1 = [q_1 \ q_2 \ q_3]^T$ .  $v(q_a, \dot{q}_a)$  and  $h(q_a)$  can be expressed as follows:

$$v(q_a, \dot{q}_a) = -\bar{M}_1^{-1}(\bar{G} + \bar{C}\dot{q}_a) \quad (7)$$

$$h(q_a) = \bar{M}_1^{-1} \quad (8)$$

### III. MAIN RESULTS

In this section, we integrate the integral sliding mode controller with optimal control theory, aligning it with the practical application of marine rotating cranes. We refine the cost function and formulate an enhanced *HJB* equation tailored to this context. Furthermore, we devise a batch neural network to approximate the *HJB* equation, culminating in the design of an optimal sliding mode controller grounded in adaptive dynamic programming (ADP).

#### A. CONTROL ALGORITHM DESIGN

##### 1) OPTIMAL FEEDBACK CONTROLLER DESIGN

The control objective of this paper is to make the following equations hold:

$$\lim_{t \rightarrow \infty} q = q_d \quad (9)$$

$$\lim_{t \rightarrow \infty} \dot{q} = \dot{q}_d \quad (10)$$

where  $q_d = [q_{1d} \ q_{2d} \ q_{3d} \ 0 \ 0]^T$  represents the expected values.

For the ship-mounted rotary crane model, we need to ensure accurate positioning of the load and pendulum angle suppression. To reduce the positioning and pendulum angle inaccuracies stemming from model uncertainties, the following sliding mode surface is devised:

$$s = \dot{e}_a + k_1 e_a + k_2 \int_0^t e_a(\tau) d\tau \quad (11)$$

where  $e_a = q_a - q_d = [q_1 - q_{1d} \ q_2 - q_{2d} \ q_3 - q_{3d}]^T$  is the error signal of the driveable variable,  $q_{1d}, q_{2d}, q_{3d}$  represent the desired localization position, and  $k_1, k_2$  are positive variable gains.

Derivation of Eq. (10) yields:

$$\dot{s} = \ddot{e}_a + k_1 \dot{e}_a + k_2 e_a = v(q_a, \dot{q}_a) + h(q_a)(\bar{u} + \bar{d}) + p \quad (12)$$

where  $p = -\ddot{q}_d + k_1 \dot{e}_e + k_2 e_a$ .

To procure the optimal feedback controller and ensure both the convergence of the designed sliding mode surface and the trajectory tracking performance, our aim is to determine the optimal solution  $u^*$  for the input  $\bar{u}$ .

We design the following performance optimization index function:

$$J(s) = \int_0^\infty Z(\bar{u}(s), s) + \psi(\Lambda^*(s))^2 dt \quad (13)$$

where  $Z(\bar{u}(s), s) = \bar{u}^T R \bar{u} + s^T Q s \geq 0$  is utility function,  $Q \in \mathbb{R}^{3 \times 3}$  and  $R \in \mathbb{R}^{3 \times 3}$  are positive definite matrices.  $\psi$  is a positive variable gain,  $\Lambda^*(s) = \frac{\partial J^*(s)}{\partial s}$  is the partial derivative of the function  $J^*(s)$  with respect to  $s$ .

The infinitesimal form of Eq. (13) can be expressed as:

$$\begin{aligned} Z(\bar{u}(s), s) + \psi(\Lambda^*(s))^2 + \Lambda(s)^T \dot{s} \\ = Z(\bar{u}(s), s) + \psi(\Lambda^*(s))^2 + \Lambda(s)^T (v(q_a, \dot{q}_a) \\ + h(q_a)(\bar{u} + \bar{d}) + p) \\ = 0 \end{aligned} \quad (14)$$

where is a nonlinear Lyapunov equation.

Then we define the *HJB* equation:

$$\begin{aligned} H(\bar{u}(s), s, \Lambda(s)) = Z(\bar{u}(s), s) + \psi(\Lambda^*(s))^2 \\ + \Lambda(s)^T (v(q_a, \dot{q}_a) + h(q_a)(\bar{u} + \bar{d}) + p) \end{aligned} \quad (15)$$

In order for  $\bar{u} = u^*$ , the *HJB* equation needs to satisfy the following form:

$$\min_{\bar{u}(s) \in \Psi} H(\bar{u}(s), s, \Lambda^*(s)) = 0 \quad (16)$$

where  $\Psi$  is the input constraint on  $\bar{u}$  and  $J^*(s)$  is the optimal performance index function,  $J^*(s)$  can be expressed as follows:

$$J^*(s) = \min_{\bar{u}(s) \in \Psi} \int_0^\infty Z(\bar{u}(s), s) + \psi(\Lambda^*(s))^2 dt \quad (17)$$

The optimal feedback control algorithm can be obtained through the policy iteration algorithm as follows:

$$u^*(s) = -\frac{1}{2} R^{-1} h(q_a)^T \Lambda^*(s) \quad (18)$$

And we have the following expression for the *HJB* equation:

$$\begin{aligned} H(u^*(s), s, \Lambda^*(s)) \\ = Z(u^*(s), s) + \psi(\Lambda^*(s))^2 \\ + \Lambda(s)^T (v(q_a, \dot{q}_a) + h(q_a)(\bar{u} + \bar{d}) + p) = 0 \end{aligned} \quad (19)$$

## 2) PERFORMANCE INDEX FUNCTION APPROXIMATION

For the linear systems, the HJB equation outlined in Eq. (15) simplifies into the Riccati equation, rendering the problem of finding the optimal solution akin to a linear quadratic regulator problem, which is comparatively more tractable. However, for the nonlinear system under consideration in this paper, solving the HJB equation poses significant challenges. As such, the prevalent approach involves employing neural network approximation methods for estimating an approximate solution.

The performance index function can be reconstructed using neural network approach as follows:

$$J(s) = W^T \zeta(s) + \iota \quad (20)$$

where  $W \in \mathbb{R}^n$  is the weight of the neural network,  $n$  is the number of hidden layers of the neural network.  $\zeta(s) \in \mathbb{R}^n$  is the activation function, and  $\iota$  is the approximate residual. The derivation of  $J(s)$  leads to:

$$\Lambda(s) = (\Delta\zeta(s))^T W + \Delta\iota \quad (21)$$

where  $\Delta\zeta(s) = \frac{\partial\zeta(s)}{\partial s}$  is the gradient of the activation function. Next in order to complete the derivation, substituting Eq. (21) into Eq. (14):

$$\begin{aligned} Z(\bar{u}(s), s) + ((\Delta\zeta(s))^T W + \Delta\iota)^T \dot{s} \\ + \psi((\Delta\zeta(s))^T W + \Delta\iota)^T ((\Delta\zeta(s))^T W + \Delta\iota) = 0 \end{aligned} \quad (22)$$

From this, the HJB equation can also be expressed as:

$$\begin{aligned} H(\bar{u}(s), s, W) = Z(\bar{u}(s), s) + \psi((\Delta\zeta(s))^T W + \Delta\iota)^T \\ \times ((\Delta\zeta(s))^T W + \Delta\iota) + ((\Delta\zeta(s))^T W)^T \dot{s} \\ - \iota_H = 0 \end{aligned} \quad (23)$$

where  $\iota_H = -\Delta\iota^T \dot{s}$  is the approaching critic neural network residuals.

The weight vector  $W$  in the HJB function is unknown, and we use a neural network to estimate the weight vector  $W$  and realize an approximation of the performance index function.

$$\hat{J}(s) = \hat{W}^T \zeta(s) \quad (24)$$

where  $\hat{J}(s)$  is an approximation of  $J(s)$ ,  $\hat{W}$  is an approximation of  $W$ , and it can be found that the gradient of  $\hat{J}(s)$  is:

$$\hat{\Lambda}(s) = (\Delta\zeta(s))^T \hat{W} \quad (25)$$

and the HJB function can be expressed as:

$$\begin{aligned} H(\bar{u}(s), s, \hat{W}) = Z(\bar{u}(s), s) + \psi((\Delta\zeta(s))^T \hat{W})^T \\ \times ((\Delta\zeta(s))^T \hat{W}) \\ + ((\Delta\zeta(s))^T \hat{W})^T \dot{s} \end{aligned} \quad (26)$$

Define the error value of the weight vector estimate of the neural network as:

$$\tilde{W} = W - \hat{W} \quad (27)$$

and define the estimation error of the Hamiltonian function to be of the following form:

$$e = H(\bar{u}(s), s, \hat{W}) - H(\bar{u}(s), s, W) \quad (28)$$

The weight values in the neural network have a significant effect on the performance exponential function, and in order to achieve a better approximation of the performance exponential function, we update the weight vector  $W$  using the following adaptive law:

$$\dot{\hat{W}} = -\alpha e \phi \quad (29)$$

where  $\alpha > 0$ ,  $\phi = \Delta\zeta(s)\dot{s}$ , select  $E = \frac{1}{2}e_1^T e_1$  as the objective function of the gradient descent method for  $\zeta(s)$ .

Combining Eq. (22), Eq. (26), and Eq. (27), this gives:

$$e = \iota_H - \tilde{W}^T \phi \quad (30)$$

The derivation of Eq. (27) is obtained:

$$\dot{\tilde{W}} = \dot{W} - \dot{\hat{W}} = -\dot{\hat{W}} = \alpha e \phi = \alpha (\iota_H - \tilde{W}^T \phi) \phi \quad (31)$$

The ideal adaptive learning sliding-mode controller and adaptive learning sliding mode controller for neural network estimation can be obtained by Eqs. (16), (17) and (20):

$$u(s) = -\frac{1}{2}R^{-1}h(q_a)^T ((\Delta\zeta(s))^T W + \Delta\iota) \quad (32)$$

$$\hat{u}(s) = -\frac{1}{2}R^{-1}h(q_a)^T (\Delta\zeta(s))^T \hat{W} \quad (33)$$

## B. PROOF OF STABILITY

In this section, we will prove the boundedness of neural network algorithms and the asymptotic stability of marine rotating cranes using Lyapunov techniques and LaSalle's invariance principle.

*Theorem 1:* The performance index function of Eq. (20) is approximated by Eq. (24), the weight vector estimation error  $\tilde{W}$  is eventually bounded under the weight vector update rate Eq. (29).

*Proof:* The following Lyapunov candidate functions are chosen:

$$V_w(t) = \frac{1}{2\alpha} \tilde{W}^T \tilde{W} \quad (34)$$

Deriving Eq. (34) and substituting Eq. (29) into it results in:

$$\begin{aligned} \dot{V}_w(t) &= \frac{1}{2\alpha} \dot{\tilde{W}}^T \tilde{W} + \frac{1}{2\alpha} \tilde{W}^T \dot{\tilde{W}} = \frac{1}{\alpha} \tilde{W}^T \dot{\tilde{W}} \\ &= \frac{1}{\alpha} \tilde{W}^T \alpha (\iota_H - \tilde{W}^T \phi) \phi = \tilde{W}^T (\iota_H - \tilde{W}^T \phi) \phi \\ &= \tilde{W}^T \iota_H \phi - (\tilde{W}^T \phi)^2 \\ &\leq -\frac{1}{2} ((\tilde{W}^T \phi)^2 - \iota_H^2) \\ &\leq -\frac{1}{2} (\iota \|\tilde{W}\|^2 - \bar{\iota}_H^2) \end{aligned} \quad (35)$$

where  $\iota$  is a positive number and satisfies  $0 < \iota < \psi_{\min}(\phi^T \phi)$  and  $\bar{\iota}_H$  is an upper bound for  $\iota_H$ . If  $\tilde{W} > \sqrt{\frac{\bar{\iota}_H^2}{\iota}}$ , then  $V_w(t)$  will

continue to decrease until  $\tilde{W} \leq \sqrt{\frac{\tilde{t}_H^2}{t}}$ . Thus  $\tilde{W}$  is eventually bounded, and the proof of **Theorem 1** is completed.

*Theorem 2:* For the ship-mounted rotary crane system shown in Eq. (1), the control of the adaptive learning sliding mode controller in Eq. (33) results in the system being asymptotically stabilized at the rate of weight update in Eq. (29).

*Proof:* Given the following Lyapunov candidate function:

$$V(t) = \Lambda^*(s) \quad (36)$$

Deriving Eq. (36) results in:

$$\dot{V}(t) = (\Lambda^*(s))^T (v(q_a, \dot{q}_a) + h(q_a)(u^* + \bar{d}) + p) \quad (37)$$

Substituting the optimal feedback controller in Eq. (18) into Eq. (14):

$$\begin{aligned} & s^T Qs + \frac{1}{4}(\Lambda^*(s))^T h(q_a)R^{-1}RR^{-1}h(q_a)^T \Lambda^*(s) \\ & + \psi(\Lambda^*(s))^2 + \Lambda(s)^T (v(q_a, \dot{q}_a) + h(q_a)\bar{d} + p) \\ & - \frac{1}{2}\Lambda(s)^T v(q_a)R^{-1}h(q_a)^T \Lambda^*(s) = 0 \end{aligned} \quad (38)$$

Deforming Eq. (38), we have

$$\begin{aligned} & \Lambda(s)^T (v(q_a, \dot{q}_a) + h(q_a)\bar{d} + p) = \\ & -s^T Qs - \frac{1}{4}(\Lambda^*(s))^T v(q_a)R^{-1}RR^{-1}v(q_a)^T \Lambda^*(s) \\ & - \psi(\Lambda^*(s))^2 + \frac{1}{2}\Lambda(s)^T v(q_a)R^{-1}v(q_a)^T \Lambda^*(s) \end{aligned} \quad (39)$$

Substituting Eq. (39) into Eq. (37) yields:

$$\begin{aligned} \dot{V}(t) &= (\Lambda^*(s))^T (v(q_a, \dot{q}_a) + p) + (\Lambda^*(s))^T v(q_a)(u^* + \bar{d}) \\ &= -s^T Qs - \frac{1}{4}(\Lambda^*(s))^T h(q_a)R^{-1}RR^{-1}h(q_a)^T \Lambda^*(s) \\ &\quad - \psi(\Lambda^*(s))^2 - (\Lambda(s))^T h(q_a)(u^* - \hat{u}) \end{aligned} \quad (40)$$

Substituting Eq. (31) and Eq. (32) into Eq. (40):

$$\begin{aligned} \dot{V}(t) &= -s^T Qs - \frac{1}{4}(\Lambda^*(s))^T h(q_a)R^{-1}RR^{-1}h(q_a)^T \Lambda^*(s) \\ &\quad - \psi(\Lambda^*(s))^2 + \frac{1}{2}(\Lambda(s))^T h(q_a)R^{-1}h(q_a)^T ((\Delta\zeta(s))^T W \\ &\quad + \Delta t) - (\Delta\zeta(s))^T \hat{W} \\ &= -s^T Qs - \frac{1}{4}(\Lambda^*(s))^T h(q_a)R^{-1}RR^{-1}h(q_a)^T \Lambda^*(s) \\ &\quad - \psi(\Lambda^*(s))^2 + \frac{1}{2}((\Delta\zeta(s))^T W + \Delta t)^T h(q_a)R^{-1}h(q_a)^T \\ &\quad ((\Delta\zeta(s))^T \tilde{W} + \Delta t) \end{aligned} \quad (41)$$

Let  $I = \frac{1}{2}((\Delta\zeta(s))^T W + \Delta t)^T h(q_a)R^{-1}h(q_a)^T ((\Delta\zeta(s))^T \tilde{W} + \Delta t)$  then:

$$\begin{aligned} I &= \frac{1}{2}((\Delta\zeta(s))^T W + \Delta t)^T h(q_a)R^{-1}h(q_a)^T ((\Delta\zeta(s))^T \tilde{W} + \Delta t) \\ &\leq \frac{1}{2}((\Delta\zeta(s))^T W + \Delta t)^T h(q_a)R^{-1}h(q_a)^T ((\Delta\zeta(s))^T W + \Delta t) \\ &\leq \frac{1}{2}(\Lambda^*(s))^T h(q_a)R^{-1}h(q_a)^T (\Lambda^*(s)) \end{aligned}$$

$$\begin{aligned} &\leq \left\| \frac{1}{2}(\Lambda^*(s))^T h(q_a)R^{-1}h(q_a)^T (\Lambda^*(s)) \right\| \\ &\leq \nu \end{aligned}$$

where  $\nu$  is the upper limit of  $\|\frac{1}{2}(\Lambda^*(s))^T h(q_a)R^{-1}h(q_a)^T (\Lambda^*(s))\|$ .

Since  $R$  is a positive definite matrix, we can obtain:

$$\begin{aligned} &\frac{1}{4}(\Lambda^*(s))^T h(q_a)R^{-1}RR^{-1}h(q_a)^T \Lambda^*(s) \\ &= \frac{1}{4}(\Lambda^*(s))^T h(q_a)R^{-1}h(q_a)^T \Lambda^*(s) \geq 0 \end{aligned} \quad (42)$$

Obviously,  $\psi(\Lambda^*(s))^2 \geq 0$ , combining Eqs. (41) and (42), we obtain an upper bound on  $\dot{V}(t)$ :

$$\begin{aligned} \dot{V}(t) &\leq -s^T Qs + \frac{1}{2}((\Delta\zeta(s))^T W + \Delta t)^T h(q_a)R^{-1}h(q_a)^T \\ &\quad ((\Delta\zeta(s))^T \tilde{W} + \Delta t) \\ &\leq -\psi_{\min}(Q)s^2 + \nu \end{aligned} \quad (43)$$

where  $-\psi_{\min}$  is the minimum eigenvalue of the matrix  $Q$ .

For Eq. (43), if  $\|s\| > \frac{\nu}{\psi_{\min}(Q)}$ , then  $\dot{V}(t) < 0$ , and ultimately  $s$  converges to the set  $\Omega_2 : \|s\| \leq \frac{\nu}{\psi_{\min}(Q)}$ . And because of  $V(t) \leq V(0)$  and  $V(0) \in l\infty$ , it follows that  $V(t) \in l\infty$ . Further we can get  $s \in l\infty$ ,  $e_a, \dot{e}_a \in l\infty$ .

Next a set  $\Omega = \{(q_a, \dot{q}_a) | \dot{V}(t) = 0\}$  is defined, and  $S$  is the maximal invariant set of  $\Omega$ .

From Eq. (38), we have

$$\dot{s} = 0 \Rightarrow e_a = 0, \dot{e}_a = 0 \Rightarrow q_a = 0, \dot{q}_a = 0$$

Combined with Eq. (1), this yields:

$$\begin{aligned} q_1 = 0, q_2 = 0, q_3 = 0, q_4 = 0, q_5 = 0, \\ \dot{q}_1 = 0, \dot{q}_2 = 0, \dot{q}_3 = 0, \dot{q}_4 = 0, \dot{q}_5 = 0. \end{aligned}$$

The proof of **Theorem 2** is completed.

## IV. RESULTS AND DISCUSSION

In the previous section, we proved the convergence of the proposed method theoretically and in this section the performance of the proposed method will be further verified through experiments. To assess its effectiveness, we conducted comparative experiments referencing the proposed controllers against the linear quadratic regulator (LQR) and traditional sliding mode control (SMC) on the experimental platform.

### A. EXPERIMENTAL PLATFORM AND EXPERIMENTAL PARAMETERS

We validate the methods in this paper using the experiment platform shown in FIGURE 2 used the following S-shaped trajectory as the target trajectory in this section:

$$\chi(i)_r = \begin{cases} (\chi(i)_h - \chi(i)_0) \left( \frac{t}{t_h} - \frac{\sin(\frac{2\pi t}{t_h})}{2\pi} \right) + \chi(i)_0, & t \in [0, t_h) \\ \chi(i)_h, & t \in [t_h, t_d] \end{cases} \quad (44)$$

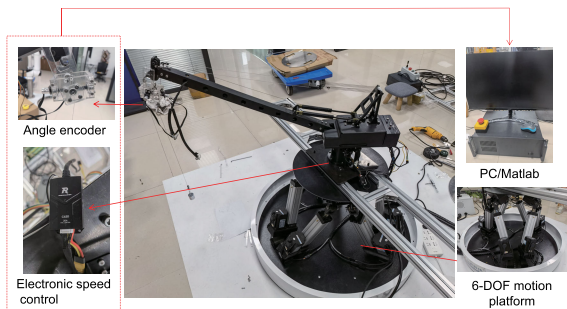


FIGURE 2. Experiment platform.

The values of the parameters used during the experiment are as follows, where  $M = 2.1[\text{kg}]$ ,  $L = 0.5[\text{m}]$ , and the initial and final target angles in the undulation direction are  $0^\circ$  and  $15^\circ$ , respectively. The initial and final target angles in the direction of rotation are  $0^\circ$  and  $15^\circ$ , respectively. The variation of rope length is  $0.2[\text{m}]$ .

The proposed controller is theoretically analyzed and empirically simulated experiments to obtain the most suitable controller gain as:

$$\begin{aligned} k_1 &= 6, k_2 = 3.5, Q = [1, 0, 0; 0, 1, 0; 0, 0, 1]^T, \\ R &= 0.2[0.2, 0, 0; 0, 0.2, 0; 0, 0, 0.2]^T, \\ \alpha &= 0.001, \psi = 2, \hat{W}_0 = [1, 1, 1]^T, \end{aligned}$$

where  $\hat{W}_0$  is the initial value of weights  $W_0$ , in our experiments, we ensured that all the above parameters were constant.

### B. COMPARATIVE EXPERIMENTS

We selected the LQR controller and SMC as the comparison controller.

LQR controller is as follows:

$$\begin{aligned} \tau_1 &= -k_{11}e_1 - k_{12}\dot{e}_1 - k_{13}q_4 - k_{14}\dot{q}_4 + \tau_{1f} \\ \tau_2 &= -k_{21}e_2 - k_{22}\dot{e}_2 - k_{23}q_5 - k_{24}\dot{q}_5 + \tau_{2f} \\ \tau_3 &= -k_{31}e_3 - k_{32}\dot{e}_3 - mg + \tau_{3f} \end{aligned}$$

where  $e_1 = q_1 - q_{1d}$ ,  $e_2 = q_2 - q_{2d}$ ,  $e_3 = q_3 - q_{3d}$ ,  $k_{11} = 45$ ,  $k_{12} = 24$ ,  $k_{13} = 4.5$ ,  $k_{14} = -0.1$ ,  $k_{21} = 45$ ,  $k_{22} = 31$ ,  $k_{23} = 3.9$ ,  $k_{24} = 5.5$ ,  $k_{31} = 31$ ,  $k_{32} = 8$ .

The crane model shown in Eq. (1) is linearized as follows:

$$\begin{aligned} (mL^2 + \frac{1}{3}M_1L^2)\ddot{q}_1 - mL C_{1d}\ddot{q}_3 + mLq_{3d}S_{1d}\ddot{q}_4 \\ + (m + \frac{1}{2}M_1)(g + \ddot{h})LC_{1d} = \tau_1 \\ (\frac{1}{3}M_1L^2C_{1d}^2 + mL^2C_{1d}^2)\ddot{q}_2 + mLq_{3d}C_{1d}\dot{q}_5 = \tau_2 \\ -mL C_{1d}\dot{q}_1 + m\ddot{q}_3 - m(g + \ddot{h}) = \tau_3 \\ mLq_{3d}S_{1d}\ddot{q}_1 + mq_{3d}^2\ddot{q}_4 + m(g + \ddot{h})q_{3d}q_4 = 0 \\ mLq_{3d}C_{1d}\ddot{q}_2 + mq_{3d}^2\ddot{q}_5 + m(g + \ddot{h})q_{3d}q_5 = 0 \end{aligned}$$

The linearized equation is then deformed to obtain:

$$\ddot{q} = \beta_s + \eta_U$$

Then, we set:

$$\begin{aligned} S_1 &= e + \varphi\dot{e}, \\ \dot{S}_1 &= -\mu S_1 - \rho \tanh(S_1), \end{aligned}$$

where

$$\begin{aligned} e &= q - q_d, \\ q &= [q_1 \ q_2 \ q_3 \ q_4 \ q_5]^T \\ q_d &= [q_{1d} \ q_{2d} \ q_{3d} \ 0 \ 0]^T \\ \varphi &= \text{diag}(\varphi_1, \varphi_2, \varphi_3, \varphi_4), \varphi_5) \end{aligned}$$

The specific expressions for SMC are as follows:

$$\tau_{smc} = \eta^T [\ddot{q}_d + \varphi^T(-\mu S - \rho \tanh(S) - \dot{q} + \dot{q}_d) - \beta_s] \quad (45)$$

where  $\varphi_1 = 65$ ,  $\varphi_2 = 50$ ,  $\varphi_3 = 3$ ,  $\varphi_4 = 2$ ,  $\varphi_5 = 1.5$ ,  $\mu = 45$ ,  $\rho = 10$ .

The results from the comparative experiments are illustrated in FIGURE 3. While tracking the same reference trajectory, both the SMC and LQR controllers exhibit certain overshooting and hysteresis responses during the rising phase, contrasting with the smoother trajectory tracking demonstrated by the proposed controller. Regarding pendulum suppression, during the rising phase, the pendulum angles of the LQR and SMC controllers notably display larger oscillations compared to those of the proposed controller. After 5 seconds, the pendulum angles of the proposed controller stabilize, whereas those of the LQR and SMC controllers continue to exhibit instability. TABLE 2 shows more detailed parameters including reaching time  $t_{q1}$ ,  $t_{q2}$ ,  $t_{q3}$  and maximum swing angle  $q_{4max}$ ,  $q_{5max}$ . The jib positioning manoeuvres and rope length changes of the cranes using the proposed controllers tracked the reference trajectory better, however, the cranes using the LQR and the SMC increased the time to complete the above manoeuvres by  $-9.5^\circ, 13.9^\circ, -4.2^\circ$  and  $13.75^\circ, 19.9^\circ, -2.8^\circ$ . In terms of pendulum angle suppression, the maximum pendulum angles using the proposed controller are  $0.59^\circ$  and  $1.1^\circ$ , which are 63%, 26% and 69.9%, 61.1% lower than those of LQR and SMC, respectively. In summary, it is evident that the proposed controller yields significantly smoother pendulum trajectories compared to the SMC and LQR controllers.

Next, the robustness of the proposed controller is assessed by varying the model parameters of the ship-mounted rotary crane. When comparing the positioning effectiveness and swing angle suppression of the SMC and LQR controllers under changes in load mass and initial rope length, as depicted in FIGURES 3 and 4, it becomes evident that although the LQR and SMC controllers can achieve a relatively satisfactory positioning effect, they struggle to adequately suppress swing angles, especially when the system's model parameters and intrinsic frequency are altered. Even as the experimental duration progresses, significant swing angles persist. In contrast, the proposed controller effectively confines swing angles within a predefined range throughout the experiment's duration.

**TABLE 2. Comparative experiment results ( $m = 0.5[\text{kg}], l = 0.3[\text{m}]$ ).**

Control method	Reaching time $t_{q_1}$ [s]	Reaching time $t_{q_2}$ [s]	Reaching time $t_{q_3}$ [s]
Proposed	10.00	10.00	5.00
LQR	9.05	11.39	4.79
SMC	11.375	11.99	4.86
	Maximum value $q_{4max}$ [°]	Maximum value $q_{5max}$ [°]	
Proposed	0.59	1.1	
LQR	1.6	1.49	
SMC	1.96	2.83	

**TABLE 3. Comparative experiment results ( $m = 1[\text{kg}], l = 0.5[\text{m}]$ ).**

Control method	Reaching time $t_{q_1}$ [s]	Reaching time $t_{q_2}$ [s]	Reaching time $t_{q_3}$ [s]
Proposed	10.00	10.00	5.00
LQR	10.35	9.24	4.8
SMC	9.5	8.77	4.9
	Maximum value $q_{4max}$ [°]	Maximum value $q_{5max}$ [°]	
Proposed	0.97	0.95	
LQR	1.46	4.8	
SMC	2.0	2.56	

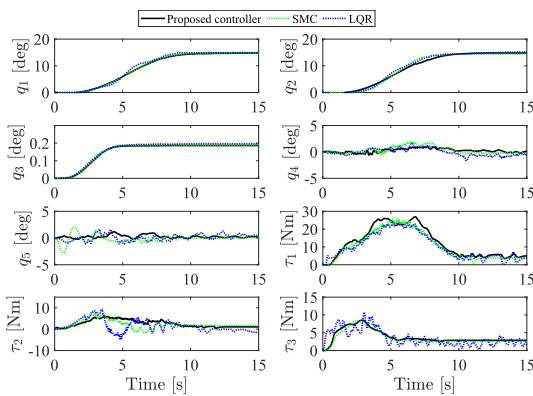


**FIGURE 3. Experimental results ( $m = 0.5[\text{kg}], l = 0.3[\text{m}]$ ).**

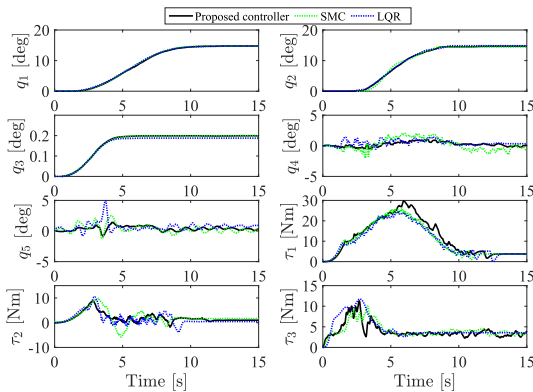


**FIGURE 4. Experimental results ( $m = 1[\text{kg}], l = 0.5[\text{m}]$ ).**

More detailed parameters are shown in TABLE 3. The crane jib positioning operations and the tracking of rope length changes to the reference trajectory using this controller remained good with changing system parameters, but the time to complete the above operations increased by 3.5°, -7.6°, -4°, and -5° for the cranes using the LQR and SMC, respectively, and -13.2°, and -2°. Similarly, the maximum swing angles using this controller are 0.97° and 0.95°, which are 33.6%, 80.2%, 51.5%, and 62.9% smaller than those of the LQR and SMC, respectively. Therefore,

the controller proposed in this paper also has a relatively excellent performance in terms of robustness.

Under both LQR and SMC,  $t_{q_1}$ ,  $t_{q_2}$  and  $t_{q_3}$  still fail to reach the predetermined time and as a result, the load swing angle becomes more jittery. Because for the q-matrix, if the LQR can only be adjusted manually by experience, which is difficult to attain good positioning effect while achieving good swing angle suppression. sgn, the sign function included in the SMC, maintains the control quantity on the surface of the sliding mode, but on the other hand it also causes the load swing angle to be existed. The controller proposed in this paper reduces the error generated in the control process by establishing the optimal performance indicator function of the sliding mode and solving the HJB equation based on the strategy iteration algorithm, which approximates the unknown function through neural network.

### V. CONCLUSION

In this paper, in order to solve the control problem of the ship-mounted rotary crane, an optimal feedback controller is proposed by combining the optimal control and sliding mode control, which achieves the precise positioning of the load and the suppression of the pendulum angle, and finally the validity of the proposed method is verified by theories and experiments.

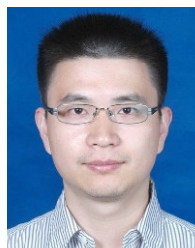
### ACKNOWLEDGMENT

The authors are indebted to the anonymous reviewers for their constructive and insightful comments.

### REFERENCES

- [1] B. Guo and Y. Chen, "Fuzzy robust fault-tolerant control for offshore ship-mounted crane system," *Inf. Sci.*, vol. 526, pp. 119–132, Jul. 2020.
- [2] F. Rauscher and O. Sawodny, "Modeling and control of tower cranes with elastic structure," *IEEE Trans. Control Syst. Technol.*, vol. 29, no. 1, pp. 64–79, Jan. 2021.
- [3] P. Cai, I. Chandrasekaran, J. Zheng, and Y. Cai, "Automatic path planning for dual-crane lifting in complex environments using a prioritized multiobjective PGA," *IEEE Trans. Ind. Informat.*, vol. 14, no. 3, pp. 829–845, Mar. 2018.

- [4] J. Huang, X. Xie, and Z. Liang, "Control of bridge cranes with distributed-mass payload dynamics," *IEEE/ASME Trans. Mechatronics*, vol. 20, no. 1, pp. 481–486, Feb. 2015.
- [5] V. D. La and K. T. Nguyen, "Combination of input shaping and radial spring-damper to reduce tridirectional vibration of crane payload," *Mech. Syst. Signal Process.*, vol. 116, pp. 310–321, Feb. 2019.
- [6] M. J. Maghsoudi, L. Ramli, S. Sudin, Z. Mohamed, A. R. Husain, and H. Wahid, "Improved unity magnitude input shaping scheme for sway control of an underactuated 3D overhead crane with hoisting," *Mech. Syst. Signal Process.*, vol. 123, pp. 466–482, May 2019.
- [7] P.-Y. Shen, J. Schatz, and R. J. Caverly, "Passivity-based adaptive trajectory control of an underactuated 3-DOF overhead crane," *Control Eng. Pract.*, vol. 112, Jul. 2021, Art. no. 104834.
- [8] H. Ouyang, X. Xu, and G. Zhang, "Boom motion trajectory generation approach for load sway rejection in rotary cranes considering double-pendulum effect," *Meas. Control*, vol. 54, nos. 5–6, pp. 924–934, May 2021.
- [9] N. Sun, Y. Fu, T. Yang, J. Zhang, Y. Fang, and X. Xin, "Nonlinear motion control of complicated dual rotary crane systems without velocity feedback: Design, analysis, and hardware experiments," *IEEE Trans. Autom. Sci. Eng.*, vol. 17, no. 2, pp. 1017–1029, Apr. 2020.
- [10] Z. Zhang, Y. Wu, and J. Huang, "Differential-flatness-based finite-time anti-swing control of underactuated crane systems," *Nonlinear Dyn.*, vol. 87, no. 3, pp. 1749–1761, Feb. 2017.
- [11] B. Lu, Y. Fang, and N. Sun, "Sliding mode control for underactuated overhead cranes suffering from both matched and unmatched disturbances," *Mechatronics*, vol. 47, pp. 116–125, Nov. 2017.
- [12] M. Zhang, X. Jing, and Z. Zhu, "Disturbance employment-based sliding mode control for 4-DOF tower crane systems," *Mech. Syst. Signal Process.*, vol. 161, Dec. 2021, Art. no. 107946.
- [13] H. Ouyang, X. Xu, and G. Zhang, "Tracking and load sway reduction for double-pendulum rotary cranes using adaptive nonlinear control approach," *Int. J. Robust Nonlinear Control*, vol. 30, no. 5, pp. 1872–1885, Mar. 2020.
- [14] H. Chen, Y. Fang, and N. Sun, "A swing constraint guaranteed MPC algorithm for underactuated overhead cranes," *IEEE/ASME Trans. Mechatronics*, vol. 21, no. 5, pp. 2543–2555, Oct. 2016.
- [15] C. Aguiar, D. Leite, D. Pereira, G. Andonovski, and I. Škrjanc, "Nonlinear modeling and robust LMI fuzzy control of overhead crane systems," *J. Franklin Inst.*, vol. 358, no. 2, pp. 1376–1402, Jan. 2021.
- [16] H. Moradi and G. Vossoughi, "State estimation, positioning and anti-swing robust control of traveling crane-lifter system," *Appl. Math. Model.*, vol. 39, no. 22, pp. 6990–7007, Nov. 2015.
- [17] J. Lu, Q. Wei, T. Zhou, Z. Wang, and F.-Y. Wang, "Event-triggered near-optimal control for unknown discrete-time nonlinear systems using parallel control," *IEEE Trans. Cybern.*, vol. 53, no. 3, pp. 1890–1904, Mar. 2023.
- [18] A. Mahajan, "Optimal decentralized control of coupled subsystems with control sharing," *IEEE Trans. Autom. Control*, vol. 58, no. 9, pp. 2377–2382, Sep. 2013.
- [19] L. Zhang, M. Liu, and B. Xie, "Optimal control of an SIQRS epidemic model with three measures on networks," *Nonlinear Dyn.*, vol. 103, no. 2, pp. 2097–2107, Jan. 2021.
- [20] Y. Jiang and Z.-P. Jiang, "Robust adaptive dynamic programming for large-scale systems with an application to multimachine power systems," *IEEE Trans. Circuits Syst. II, Exp. Briefs*, vol. 59, no. 10, pp. 693–697, Oct. 2012.
- [21] H. Zhang, J. Zhang, G.-H. Yang, and Y. Luo, "Leader-based optimal coordination control for the consensus problem of multiagent differential games via fuzzy adaptive dynamic programming," *IEEE Trans. Fuzzy Syst.*, vol. 23, no. 1, pp. 152–163, Feb. 2015.
- [22] W. Gao, Y. Jiang, and M. Davari, "Data-driven cooperative output regulation of multi-agent systems via robust adaptive dynamic programming," *IEEE Trans. Circuits Syst. II, Exp. Briefs*, vol. 66, no. 3, pp. 447–451, Mar. 2019.
- [23] Z. Ming, H. Zhang, Y. Yan, and J. Zhang, "Tracking control of discrete-time system with dynamic event-based adaptive dynamic programming," *IEEE Trans. Circuits Syst. II, Exp. Briefs*, vol. 69, no. 8, pp. 3570–3574, Aug. 2022.
- [24] F. F. M. El-Sousy, M. M. Amin, and A. Al-Durra, "Adaptive optimal tracking control via actor-critic-identifier based adaptive dynamic programming for permanent-magnet synchronous motor drive system," *IEEE Trans. Ind. Appl.*, vol. 57, no. 6, pp. 6577–6591, Nov. 2021.
- [25] F. Zhao, W. Gao, T. Liu, and Z.-P. Jiang, "Event-triggered robust adaptive dynamic programming with output feedback for large-scale systems," *IEEE Trans. Control Netw. Syst.*, vol. 10, no. 1, pp. 63–74, Mar. 2023.
- [26] D. Liu, W. Yu, S. Baldi, J. Cao, and W. Huang, "A switching-based adaptive dynamic programming method to optimal traffic signaling," *IEEE Trans. Syst., Man, Cybern. Syst.*, vol. 50, no. 11, pp. 4160–4170, Nov. 2020.
- [27] R. Wang, D. Ma, M.-J. Li, Q. Sun, H. Zhang, and P. Wang, "Accurate current sharing and voltage regulation in hybrid wind/solar systems: An adaptive dynamic programming approach," *IEEE Trans. Consum. Electron.*, vol. 68, no. 3, pp. 261–272, Aug. 2022.
- [28] R. Tang, B. Luo, and Y. Liao, "Adaptive dynamic programming based composite control for profile tracking with multiple constraints," *Neurocomputing*, vol. 557, Nov. 2023, Art. no. 126711.
- [29] H. Dong, Z. Ning, and Z. Ma, "Nearly optimal fault-tolerant constrained tracking for multi-axis servo system via practical terminal sliding mode and adaptive dynamic programming," *ISA Trans.*, vol. 144, pp. 308–318, Jan. 2024.
- [30] F. Li, L. Gao, Y. Zhang, and Y. Liu, "Hierarchical operation switch schedule algorithm for energy management strategy of hybrid electric vehicle using adaptive dynamic programming," *Sustain. Energy, Grids Netw.*, vol. 35, Sep. 2023, Art. no. 101107.
- [31] J. Na, G. Li, B. Wang, G. Herrmann, and S. Zhan, "Robust optimal control of wave energy converters based on adaptive dynamic programming," *IEEE Trans. Sustain. Energy*, vol. 10, no. 2, pp. 961–970, Apr. 2019.
- [32] Z. Wang, Y. Wang, and Z. Kowalczyk, "Adaptive optimal discrete-time output-feedback using an internal model principle and adaptive dynamic programming," *IEEE/CAA J. Autom. Sinica*, vol. 11, no. 1, pp. 131–140, Jan. 2024.
- [33] Q. Wu, H. Ouyang, and H. Xi, "Real-time trajectory planning for ship-mounted rotary cranes considering continuous sea wave disturbances," *Nonlinear Dyn.*, vol. 111, no. 22, pp. 20959–20973, Nov. 2023.



**HUAN XI** (Member, IEEE) received the B.S., M.S., and Ph.D. degrees in electrical engineering from Nanjing University of Aeronautics and Astronautics, Nanjing, China, in 2004, 2007, and 2012, respectively.



**QIANGYING WU** received the B.S. degree in electrical engineering and automation from Jiangsu University of Technology, in 2019. He is currently pursuing the M.S. degree in control engineering with Nanjing Tech University. His main research interest includes underactuated marine crane system control.



**HUIMIN OUYANG** (Senior Member, IEEE) received the B.Eng. degree in electrical engineering and automation from Tianjin Chengjian University, Tianjin, China, in 2005, the M.Eng. degree in mechatronics from Nagoya Institute of Technology, Nagoya, Japan, in 2009, and the Ph.D. degree in mechatronics from Toyohashi University of Technology, Toyohashi, Japan, in 2012.

Since 2013, he has been with the College of Electrical Engineering and Control Science, Nanjing Tech University, Nanjing, China, where he is currently a Full Professor. His major research interests include system control theory and its application to mechatronics.

• • •